FASTC-ID(RS)T-0932-92

FOREIGN AEROSPACE SCIENCE AND TECHNOLOGY CENTER

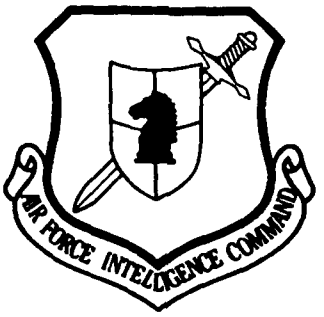

NUMERICAL SOLUTION OF SUPG FINITE-ELEMENT METHOD FOR SUPERSONIC VISCOUS FLOW

by

Xu Guoqun, Zhang Guofu

HUMAN TRANSLATION

FASTC-ID(RS)T-0932-92 20 July 1993

MICROFICHE NR: 93C000467

NUMERICAL SOLUTION OF SUPG FINITE-ELEMENT METHOD FOR SUPERSONIC VISCOUS FLOW

By: Xu Guoqun, Zhang Guofu

English pages: 18

Source: Lixue Xuebao, Vol. 23, No. 5, 1991; pp. 533-541

Country of origin: China
Translated by: Leo Kanner Associates
F33657-88-D-2188
Requester: FASTC/TATV/Paul Freisthler

PREPARED BY:

TRANSLATION DIVISION
FOREIGN AEROSPACE SCIENCE AND TECHNOLOGY CENTER
WPAFB, OHIO

GRAPHICS DISCLAIMER

All figures, graphics, tables, equations, etc. merged into this translation were extracted from the best quality copy available.

NUMERICAL SOLUTION OF SUPG FINITE-ELEMENT METHOD FOR SUPERSONIC VISCOUS FLOW

Xu Guoqun and Zhang Guofu

Nanjing Aeronautical College, Nanjing 210016

Abstract: A streamline upwind/Petrov-Galerkin (SUPG) weighted residual formalism was developed in the paper for the quasi-simplified Navier-Stokes equations. Numerical computations were made for Burger's equation, the nonviscous shock wave reflection problem, as well as supersonic laminar flow over a flat plate and compression corner flow by using the method. The results of the computations show that this method is accurate, convergent, and stable.

Key words: Navier-Stokes equations, supersonic viscous flow, finite-element method, SUPG method.

I. Introduction

When the convection flow term is present, the differential operator is nonself-adjoint; the coefficient matrix in the Galerkin method is nonsymmetric. The method lacks the advantage

of optimal approximation. Often this situation causes fluctuations in the numerical solution. For problems involving high Pe numbers or large Re numbers, this phenomenon is especially serious. To control convection of each element, the mesh can be made finer; however, in this case a large amount of internal memory will be used. In 1979, Hughes and Brooks [1] proposed the SUPG method. The method has better stability and higher accuracy, capable of effectively processing high-speed flow problems, including the problem in which the interruption plane lies in the flow plane. The present authors verified that the SUPG method and the PG (Penalty Galerkin) method developed by Baker [2] are somewhat equally effective for high-speed viscous flow problems. However, expansion and application of the SUPG method is more promising than the PG method [3]. In references [4, 5], the SUPG finite-element method is used to solve for the incompressible Navier-Stokes equation set. In reference [6], the Euler equation set is solved. However, up to now the authors did not find any report in which the SUPG finite-element method was used in solving problems of supersonic viscous flow.

II. Model Equations

Below, Burgers' equation is discussed:

$$\left.\begin{aligned} &\frac{\partial u}{\partial t} + u\frac{\partial u}{\partial x} - k\frac{\partial^2 u}{\partial x^2} = 0,\ -1 < x < 1,\ t > 0 \\ &u(0,x) = -\frac{1}{2}x,\ -1 \leqslant x \leqslant 1 \\ &u(t,-1) = 0.5,\ u(t,1) = -0.5,\ t > 0 \end{aligned}\right\} \tag{1}$$

Define the weighted function W_i in the element as

$$W_i = N_i + P_i \tag{2}$$

In the equation, N_i is the interpolation function, a C^0 function, which is continuous at the element boundary. P_i is the perturbation of the weighted function, a C^{-1} function, which is discontinuous at the element boundary. Then, we write out the Petrov-Galerkin expression form of Eq. (1) as

$$\int_\Omega \left[N_i \left(\frac{\partial u}{\partial t} + u \frac{\partial u}{\partial x} \right) - k \frac{\partial u}{\partial x} \frac{\partial N_i}{\partial x} \right] d\Omega + \sum_{e=1}^{n_{el}} \int_{\Omega^e} P_i \left(\frac{\partial u}{\partial t} + u \frac{\partial u}{\partial x} \right) d\Omega = 0 \tag{3}$$

In the equation, n_{el} is the number of elements; in this paper, the linear interpolation value is taken as u. Therefore, there is no second-order derivative term in the second integration term of Eq. (3). In the SUPG finite-element method, the perturbation P_i of the weighted function can be taken as

$$P_i = \alpha \Delta t \frac{\partial N_i}{\partial x} \tag{4}$$

Here, α is the algorithm parameter, and Δt is the duration of the time step.

Use Eq. (3) to solve for the above-mentioned problem of a specific solution. Fig. 1 shows the results of computations when $k = 10^{-4}$. Fig. 1(a) and (b) are, respectively, the results when $\alpha = 0$ and when $\alpha = 0.3$. The numerical solutions shows fluctuations upstream and downstream of the shock wave; this is a nonphysical solution, which fails to satisfies the entropy-increase condition [7] expressed in the second law of thermodynamics. Fig. 1(d) shows the solution when $\alpha = 1.0$. The solution appears as an excessive divergence in the neighborhood

of the shock wave, thus showing lower accuracy. Fig. 1(c) shows the results when $\alpha = 0.5$. At this point, the virtual fluctuation of the finite-element solution in the neighborhood of the shock altogether disappears; in addition, accuracy is also ensured.

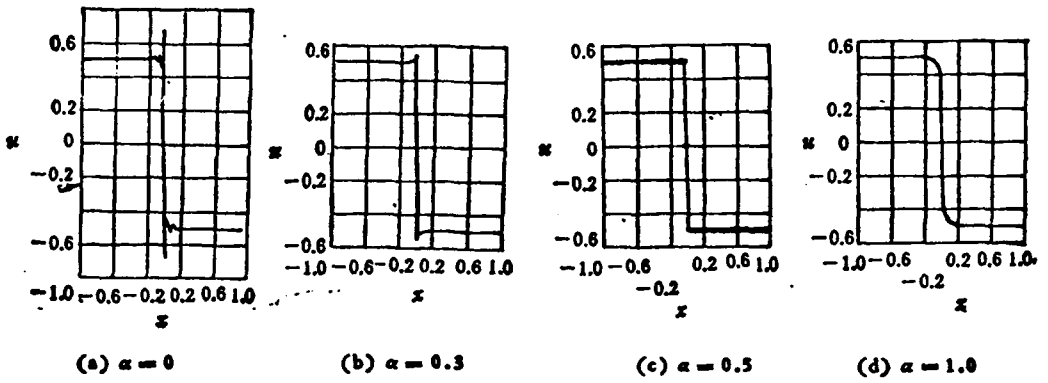

Fig. 1. Solutions of Burgers' equation when $k = 10^{-4}$ given in computations
_____ accurate solution
• -- numerical solution as given in the paper

Fig. 2(a) and (b) show, respectively, the numerical results when $k = 0$ and when $k = 10^{-2}$. From the figure, we can see that the numerical solution and the accurate solution are in good agreement. In addition, when k is less than or equal to 10^{-4}, the shock wave travels only one mesh point. The method exhibits high discriminability for a shock wave.

III. Quasi-simplified Navier-Stokes Equations and Their Variation Form

Assume that t stands for time, u and v are components of the gas flow velocity in the x and y axes. p, ρ, T, and μ are the pressure, density, temperature, and viscosity coefficients of the

gas; and ν is the adiabatic index. To simplify the computations, the second-order derivative terms in the x-direction (along the direction of the object surface) can be neglected in supersonic and hypersonic problems. Then in the case of dimensionless nonsteady state for an ideal gas at constant specific heat, the Navier-Stokes equation set can be simplified as

$$\rho \frac{\partial U}{\partial t} + A_1 \frac{\partial U}{\partial x} + A_2 \frac{\partial U}{\partial y} + \frac{\partial \sigma}{\partial y} + \phi = 0 \qquad (5)$$

Here, U, σ, and ϕ are vectors; A_1 and A_2 are the matrixes

$$U = \begin{bmatrix} \rho \\ u \\ v \\ T \end{bmatrix} \quad A_1 = \begin{bmatrix} \rho u & \rho^2 & 0 & 0 \\ \dfrac{T}{\nu M_\infty^2} & \rho u & 0 & \dfrac{\rho}{\nu M_\infty^2} \\ 0 & 0 & \rho u & 0 \\ 0 & (\nu - 1)\rho T & 0 & \rho u \end{bmatrix}$$

$$\sigma = \begin{bmatrix} \sigma_1 \\ \sigma_2 \\ \sigma_3 \\ \sigma_4 \end{bmatrix} \quad A_2 = \begin{bmatrix} \rho v & 0 & \rho^2 & 0 \\ 0 & \rho v & 0 & 0 \\ \dfrac{T}{\nu M_\infty^2} & 0 & \rho v & \dfrac{\rho}{\nu M_\infty^2} \\ 0 & 0 & (\nu - 1)\rho T & \rho v \end{bmatrix}.$$

$$\sigma_1 = 0, \qquad \sigma_2 = -\frac{\mu}{\mathrm{Re}_{\infty L}} \frac{\partial u}{\partial y}$$

$$\sigma_3 = -\frac{4}{3} \frac{\mu}{\mathrm{Re}_{\infty L}} \frac{\partial v}{\partial y}, \quad \sigma_4 = -\frac{\nu \mu}{\mathrm{Re}_{\infty L} \mathrm{Pr}} \frac{\partial T}{\partial y}$$

$$\phi = [\phi_1, \phi_2, \phi_3, \phi_4]^T$$

$$\phi_1 = \phi_2 = \phi_3 = 0$$

$$\phi_4 = -\frac{1}{C_v} \frac{\mu}{\mathrm{Re}_{\infty L}} \left[\frac{4}{3} \left(\frac{\partial v}{\partial y} \right)^2 + \left(\frac{\partial u}{\partial y} \right)^2 \right]$$

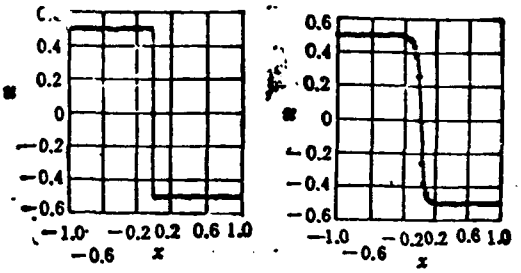

(a) $t = 0$ (b) $t = 10^{-2}$

Fig. 2. Calculated solutions of Burgers' equation when $\alpha = 0.5$
_____ accurate solution ● - numerical solution as given in the paper

To bring the equation set to a closure, the state equation and the viscosity law equation should be added. The state equation is

$$p = \frac{1}{\gamma M_\infty^2} \rho T \tag{6}$$

There is also the constant-volume specific heat equation, $C_v = p_\infty/(\gamma - 1)$. The viscosity equation adopts the Sutherland relationship

$$\mu = T^{3/2} \frac{1 + S'/T'_\infty}{T + S'/T'_\infty} \tag{7}$$

In the above-mentioned equation, $Re_{\infty L}$ is the Reynolds number of the incoming flow, and Pr is the Prandtl number (taken as 0.72 in the paper). When calculating μ, $S' = 114K$.

The weak solution is taken for Eq. (5). In addition, Green's formula is used, thus we establish the variation equation in the following form:

$$\int_{\Omega}\left[N_i I\left(\rho\frac{\partial U}{\partial t}+A_1\frac{\partial U}{\partial x}+A_2\frac{\partial U}{\partial y}+\phi\right)-\sigma\frac{\partial N_i}{\partial y}\right]d\Omega$$

$$+\sum_{i=1}^{n+1}\int_{\Omega'}P_i\left(\rho\frac{\partial U}{\partial t}+A_1\frac{\partial U}{\partial x}+A_2\frac{\partial U}{\partial y}+\phi\right)d\Omega$$

$$-\oint_{\Gamma}N_i\sigma dx \tag{8}$$

In Eq. (8), I is the 4 x 4 element matrix. N_i is the fundamental function of the interpolation value, which is continuous at each element boundary. In the paper, the interpolation values of four nodal points are taken for ρ, u, v, and T:

$$U=\sum_{i=1}^{4}N_iU_i \tag{9}$$

Assume that the natural boundary conditions are homogeneous in Eq. (8) for spatial divergence. We have the semi-divergence finite-element equation

$$M\dot{U}+(C+F)U=0 \tag{10}$$

In the equation, M = M(U,t), which is the mass matrix. C = C(U,t), which is the rigidity matrix (or the convection matrix). F is the divergence matrix; and U is the derivative of U with respect to time. The matrix in Eq. (10) is the aggregation of each element.

IV. Selection of Perturbation of Weighted Function

In the SUPG finite-element method, the perturbation P_i of a weighted function is related to the fraction matrix of the first-order derivative terms. Now, P_i is written as

$$P_i = \tau\left(A_1 \frac{\partial N_I}{\partial x} + A_2 \frac{\partial N_I}{\partial y}\right) \qquad (11)$$

In the equation, $\tau \cdot A_1$, and $\tau \cdot A_2$ are, respectively, the artificial viscosity coefficients along the x and y directions. In the paper, τ is taken as related to the duration of the time step. Experience with computations proves that this approach is effective.

$$\tau = \alpha \cdot \Delta t \qquad (12)$$

In the equation, α is the algorithm parameter. There are different values to be taken for equation sets of different kinds. According to reference [6], the steady-state time-step duration Δt of the entire computation can be estimated by using the following equation.

$$\Delta t = \min_{e,i}(10h_i^e/a_i) \quad \text{(not solving for the sum)} \qquad (13)$$

In the equation, the subscript i indicates the coordinate direction; the superscript e indicates the compilation number of the elements; h_i^e is the length of element e along the direction x_i (refer to Fig. 3); a_i is the spectrum radius of A (the maximum absolute value for the characteristic value).

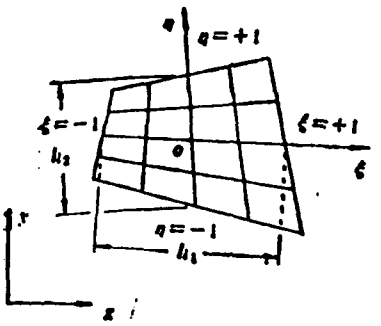

Fig. 3. Finite element of equal parameters

V. Estimation and Revision Algorithm

Write out Eq. (10) as the all-implicit form

$$M^{(i)}_{n+1}\alpha^{(i)}_{n+1} + C^{(i)}_{n+1}U^{(i)}_{n+1} = 0 \tag{14}$$

In the above equation, the subscript is the time step and the superscript is the number of iterative substitutions of the corresponding time step $\alpha^{(i)}_{n+1} = \dot{U}^{(i)}_{n+1}$. Now let us assume

$$\Delta\alpha = \alpha^{(i+1)}_{n+1} - \alpha^{(i)}_{n+1} \tag{15}$$

and assume that β is the relaxation factor. Then Eq. (14) can be written as

$$M^*\Delta\alpha = R \tag{16}$$

In the equation

$$M^* = M^{(i)}_{n+1} + \beta\Delta t(C^{(i)}_{n+1} + F^{(i)}_{n+1}) \tag{17}$$

$$R = -M^{(i)}_{n+1}\alpha^{(i)}_{n+1} - (C^{(i)}_{n+1} + F^{(i)}_{n+1})U^{(i)}_{n+1} \tag{18}$$

We can see from Eq. (16) that if M* is considered as mass and R is the driving force, then $\Delta\alpha$ corresponds to acceleration. The iterative substitution of each time step ensures the phase

equilibrium between inertial force and driving force. Also from Eq. (18) we know that if a convergent solution exists at a time step, then driving force R should gradually approach zero (the residue approaches zero) with the process of iterative substitution; therefore, the acceleration $\Delta\alpha$ also gradually tends to zero.

By combining Eqs. (15) and (16), we have the following estimation-revision algorithm:

(1) $i = 0$ (i 是迭代计数) a

(2) $U_{t+1}^{(0)} = U_t + \Delta t(1-\beta)a_t$ } (预估阶段) b

(3) $a_{t+1}^{(0)} = 0$ }

(4) $R = -M_{t+1}^{(0)}a_{t+1}^{(0)} - C_{t+1}^{(0)}U_{t+1}^{(0)}$ (残余力) c

(5) $M^*\Delta a = R$ }

(6) $a_{t+1}^{(i+1)} = a_{t+1}^{(i)} + \Delta a$ } (校正阶段) d

(7) $U_{t+1}^{(i+1)} = U_{t+1}^{(i)} + \beta\Delta t\Delta a$ }

KEY: a - (i is the number of iterative substitution)
b - (estimation stage)
c - (residual force)
d - (revision stage)

If a further step of iterative substitution is required, the computation returns to step 4. In this paper, the nonsymmetric linear equation sets are found by using this algorithm; the wave matrix technique is used to solve the equation sets. The condition for convergence for each time step is

$$\max|R| < \varepsilon_1 \qquad (19)$$

$\varepsilon_1 = 10^{-4}$. Since there is an estimation stage, generally speaking the revision times are not many, only three or four times to satisfy Eq. (19). A method with too many revision times is not desirable. When the number of revision times is too many,

the time step duration should be shortened.

The convergence criterion for the entire solving process is

$$\max \left| \frac{U_{n+1} - U_n}{U_n} \right| < \varepsilon_2 \tag{20}$$

In the equation $\varepsilon_2 = 10^{-3}$.

When the initial field is under consideration in the paper, the physical values at the boundary points are taken as given values. Thus, the inherent boundary condition of step 5 becomes

$$\Delta\alpha = 0 \tag{21}$$

VI. Computation Examples and Discussion

Since the convection terms in Eq. (8) are not separately integrated, mention of the natural boundary conditions of the exit boundary is appropriate. In the following computation examples, all conditions at the exit boundary are taken as

$$\frac{\partial f}{\partial x} = 0, \text{ 其中 } f = \rho, u, v, T \tag{22}$$

1. Reflection of nonviscous shock wave at solid wall

As one of the computation examples, in the paper the shock wave reflection problem is the first to be calculated (Mach number of incoming flow M_∞ = 2.9, and the included angle between the incident direction and the horizontal direction is 29°). In the computations, the number of elements is 44 x 11; the homogeneous flowfield is the initial condition.

Fig. 4. Equal-Mach-number curves for shock reflection at solid wall $M_\infty = 2.9$, $\Delta M = 0.0666$

Fig. 4 shows the distribution of equal-Mach-number curves found by computation; the figure clearly exhibits the incident and the reflection shock waves. Fig. 5 shows the pressure distribution at y = 0.5 given in the computations. In three zones, all the results in the paper are quite consistent with the accurate solution. The shock wave positions from the computations are slightly to the rearward compared to those in reference [7].

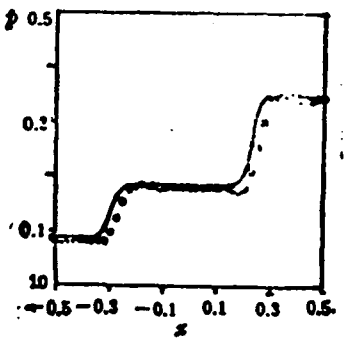

Fig. 5. Pressure distribution at y = 0.5
O - results given in the paper
___ - reference [8]

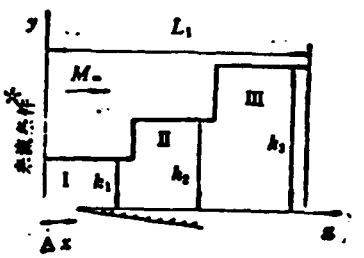

Fig. 6. Region of computation
KEY: * - conditions of incoming flow

2. Flat-plate laminar flow

Fig. 6 shows the region of solution. In the combining layer zone at the front fringe of the flat plate, the velocity drift and temperature jump are neglected. Thus, the boundary conditions of the entire wall surface at y = 0 can be written as

$$\left.\begin{aligned} u &= v = 0 \\ T &= T_w = 1 + \frac{\gamma - 1}{2} M_\infty^2 \end{aligned}\right\} \qquad (23)$$

In the equation, the wall surface temperature is taken as the total temperature of the free incoming flow.

Fig. 7 shows the pressure distribution at the wall surface. We can see from the figure that the results of computation in the paper are relatively consistent with the results given by the weak interference theory in reference [8]; in addition, there is no fluctuation phenomenon in the numerical solution at the front fringe of the flat plate. As revealed in the numerical experiments, at the front fringe of the flat plate when the step-duration Reynolds number $Re_{\Delta x} < 50$, there is no fluctuation in the numerical solution.

Fig. 8 shows the velocity and temperature profiles at x/L = 1.0. From the figure, we can see that the boundary layer is approximately at y/L = 0.25, and the front-edge shock wave is approximately sited at y/L = 0.57. This conclusion is to be expected. x/L = 1.0 is sited downstream of the front-fringe combined layer. Strong interference disintegrates as weak interference. In Fig. 8(b), the negative temperature gradient is exhibited in the neighborhood of the wall surface. This indicates heat absorption is needed from the wall surface. Given

by Eq. (23), the wall surface temperature is the total temperature of free flow as the adiabatic wall temperature when Pr = 1. However, in the case of air with Pr = 0.72, the restoration coefficient R is always smaller than 1. In other words, the adiabatic wall temperature should be smaller than the wall temperature given in Eq. (23). Therefore, in this case the flat plate should serve as the adiabatic wall surface.

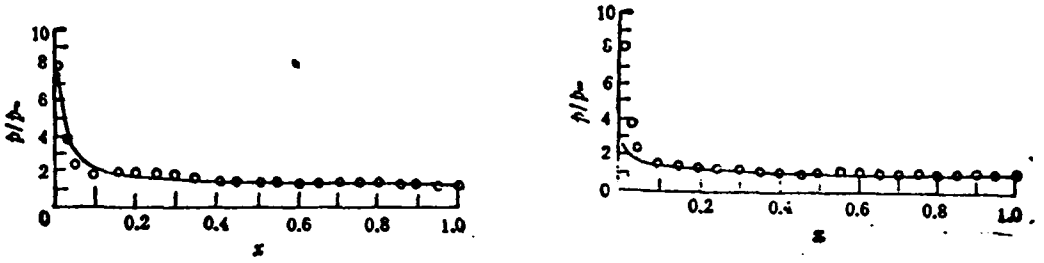

Fig. 7. Pressure distribution at wall surface
LEGEND: O - results in the paper
____ - reference [9]

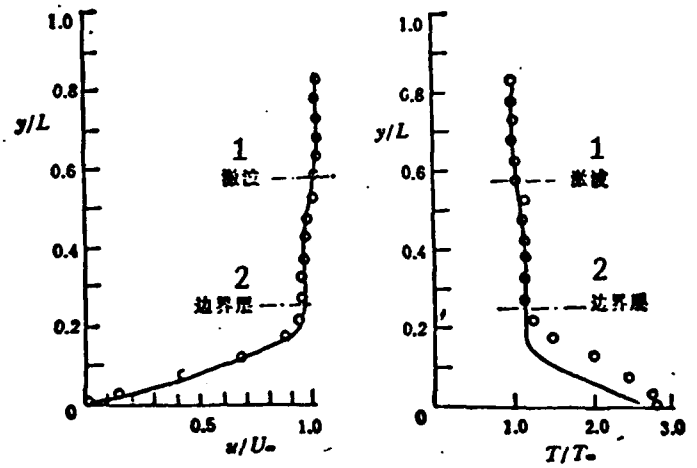

Fig. 8. Parameter profile for the case when $Re_{\infty L}$ = 1000 at x = 0.1
LEGEND: o - results in the paper
____ - reference [10]
(a) Velocity distribution (b) - Temperature distribution
KEY: 1 - shock wave 2 - boundary layer

We also see from Fig. 8 that the velocity distribution from the computations in the paper are in relatively close agreement with the values in [9]. However, the temperature distribution shows certain discrepancies within the boundary layer. On the one hand, this is because the distribution rule of wide-direction density in the vicinity of the wall surface described in reference [9] makes specifications; on the other hand, this is because only the viscosity terms that are larger than the magnitude of $O(Re_L^{-1/2})$ are retained in the quasi-simplified Navier-Stokes equation set used in this paper. Obtained from this form of the equation set, the temperature distribution in the vicinity of the wall surface often shows larger discrepancies from the solution obtained from the entire Navier-Stokes equation set.

3. Supersonic compression corner laminar flow

The foregoing method is used in the paper to calculate the flow at the two-dimensional compression corner flow of $M_\infty = 3$ and $Re_{\infty L} = 6 \times 10^5$. Fig. 9 shows the region of solution of the problem; the boundary conditions of the wall surface are shown in Eq. (23).

In the paper, the position of the left boundary is located at x = 0.3571; the physical value at the boundary is taken from the computation result of flat-plate flow mentioned previously. The number of matched points is 35 x 26; the matching mesh along the x and y directions is equally spaced, respectively, at x = 0.0428 and y = 0.0035.

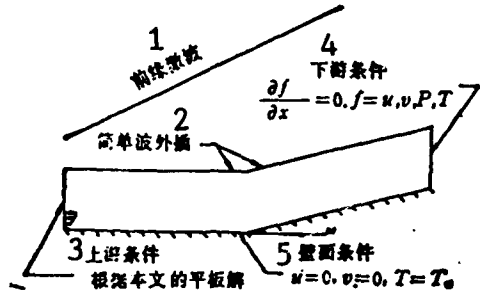

Fig. 9. Region of solution and boundary for compression corner supersonic flow
KEY: 1 - Front edge shock wave 2 - Extrapolation of simple wave 3 - Upstream condition is based on the flat-plate solution in the paper 4 - Downstream condition 5 - Wall surface condition

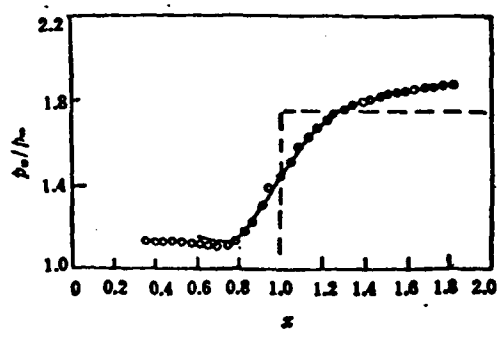

Fig. 10. Wall surface pressure distribution when $\omega = 7.5°$
LEGEND: O - results in the paper
_____ - r .erence [10] - - - - nonviscous accurate solution

Fig. 10 shows the wall surface pressure distribution obtained from computation when $\omega = 7.5°$. For comparison, the figure also shows the numerical results of Carter's difference

method [9]. From the figure we can see that the pressure continues to drop within a certain distance beginning from the left boundary. This indicates that the influence of the upstream has been taken into account. Because of the loss due to a shock wave of a nonviscous flow, the wall surface pressure of the downstream region thus calculated is higher than the nonviscous flow pressure.

VII. Conclusions

In the paper, the SUPG finite-element method is developed and applied to computations of supersonic viscous flow in obtaining relatively satisfactory numerical results. From the computations in one-dimensional and two-dimensional problems, the SUPG method certainly can restrict the fluctuations in a shock wave both downstream and upstream. However, there is a problem of selecting the free parameters. Therefore, it is necessary that we further develop the finite-element format of nonfree parameters that do not show fluctuations.

The first draft of the paper was publicly read at the Fifth Session of the All-China Computational Fluid Mechanics Conference in April 1990, at Huangshan Mountain. Xu Guoqun is currently working at the Jiangsu Provincial Investment Corporation. The paper was received for publication on 4 September 1990.

REFERENCES

1. Hughes, T. J. R. et al, AMD (ASME, New York), 1979, p. 34.

2. Baker, A. J., Comp. Meth. Appl. Mech. Eng. 51: 395-420 (1985).

3. Xu Guoqun and Zhang Guofu, Fourth Session of the Transportation Systems Symposium Between Space and Earth, Nanjing, 1988 (in press: Kongqi Dongli Xuebao [Aerodynamics])

4. Brooks, A. N. et al., Comp. Mech. Appl. Mech. Eng. 32: 199-259 (1982).

5. Xu Guoqun and Zhang Guofu, Fourth Session of the All-China Computational Fluid Mechanics Symposium, Nanjing, 1989 (in press: Kongqi Dongli Xuebao [Aerodynamics]).

6. Hughes, T. J. R., et al, Comp. Meth. Appl. Mech. Eng. 45: 217-284 (1984).

7. Zhang Hanxin, Kongqi Dongli Xuebao, 6/2, 143-165 (1988).

8. Truitt, R. W. Fundamentals of Aerodynamic Heating, The Ronald Press Company, New York, 1960.

9. Carter, J. E., NASA TR R-385.

DISTRIBUTION LIST

DISTRIBUTION DIRECT TO RECIPIENT

ORGANIZATION	MICROFICHE
B085 DIA/RTS-2FI	1
C509 BALLOC509 BALLISTIC RES LAB	1
C510 R&T LABS/AVEADCOM	1
C513 ARRADCOM	1
C535 AVRADCOM/TSARCOM	1
C539 TRASANA	1
Q592 FSTC	4
Q619 MSIC REDSTONE	1
Q008 NTIC	1
Q043 AFMIC-IS	1
E051 HQ USAF/INET	1
E404 AEDC/DOF	1
E408 AFWL	1
E410 ASDIC/IN	1
E411 ASD/FTD/TTIA	1
E429 SD/IND	1
P005 DOE/ISA/DDI	1
P050 CIA/OCR/ADD/SD	2
1051 AFIT/LDE	1
P090 NSA/CDB	1
2206 FSL	1

Microfiche Nbr: FTD93C000467
FTD-ID(RS)T-0932-92